TUDelft

Delft University of Technology

Verification and Validation of Immersed Boundary Solvers for Hypersonic Flows with Gas-Surface Interactions

Başkaya, A.O.; Capriati, Michele Capriati; Ninni, Davide ; Bonelli, Francesco ; Pascazio, Giuseppe ; Turchi, Alessandro ; Magin, Thierry; Hickel, S.

Important note
To cite this publication, please use the final published version (if applicable).
Please check the document version above.

Verification and Validation of Immersed Boundary Solvers for Hypersonic Flows with Gas-Surface Interactions

Ata O. Başkaya*

Aerodynamics Group, Faculty of Aerospace Engineering, TU Delft, The Netherlands

Michele Capriati†

Aeronautics and Aerospace Department, von Karman Institute for Fluid Dynamics, Belgium
Inria, Centre de Mathématiques Appliquées, Ecole Polytechnique, IPP, France

Davide Ninni‡, Francesco Bonelli§, and Giuseppe Pascazio¶

Dipartimento di Meccanica, Matematica & Management, Politecnico di Bari, Italy

Alessandro Turchi‖ and Thierry Magin**

Aeronautics and Aerospace Department, von Karman Institute for Fluid Dynamics, Belgium

Stefan Hickel ††

Aerodynamics Group, Faculty of Aerospace Engineering, TU Delft, The Netherlands

During atmospheric entry, the flow environment around capsules or space debris is characterized by complex fluid thermochemistry and gas-surface interactions (GSI). Computational fluid dynamics (CFD) simulations of these conditions are crucial in the design process of such objects. A promising approach for the simulation of complex geometries is the use of immersed boundary methods (IBM) and adaptive mesh refinement techniques (AMR). These methods offer reliable and efficient mesh generation and adaptation with minimal user intervention. To that end, this paper presents the recent developments of two IBM-AMR solvers coupled with the same external thermochemistry library for the accurate modelling of such complex flows including GSI. Several verification and validation cases are presented, which demonstrate the performance of the solvers. Results are analyzed in comparison with a body-conforming solver that uses the same thermochemistry library to achieve a consistent assessment of the underlying numerical methods. A good agreement between all the solvers is indicated with certain discrepancies arising due to the differences in surface treatments.

I. Introduction

Hypersonic flows experienced during atmospheric entry of capsules or space debris are characterized by strong shock waves and high-temperature effects. These conditions induce thermochemical nonequilibrium in the flow through the excitation of the internal energy modes of species and rapid chemical reactions. As the hot flow approaches the spacecraft, it begins to interact with the surface material. Depending on the characteristics of this material, these gas-surface interactions (GSI) involve catalysis as well as ablation. The latter process alleviates the heat load by means of physicochemical decomposition and mass loss, which alters the shape of the object as the surface recesses. Understanding these interactions is crucial for predicting the surface stresses and heat fluxes. Ground testing is indispensable for validation purposes; however, it is inadequate for simultaneously replicating all aspects of atmospheric entry flows. Hence, computational modelling is essential for the efficient aerothermodynamic design of future spacecraft.

*Ph.D. Candidate, Faculty of Aerospace Engineering, A.O.Baskaya@tudelft.nl

†Ph.D. Candidate, Aeronautics & Aerospace Department, michele.capriati@vki.ac.be.

‡Ph.D. Candidate, Dipartimento di Meccanica, Matematica & Management, davide.ninni@poliba.it.

§Research Fellow, Dipartimento di Meccanica, Matematica & Management, francesco.bonelli@poliba.it.

¶Professor, Dipartimento di Meccanica, Matematica & Management, giuseppe.pascazio@poliba.it.

‖Research Engineer, Aeronautics & Aerospace Department, turchi@vki.ac.be.

**Professor, Aeronautics & Aerospace Department, thierry.magin@vki.ac.be.

††Professor, Faculty of Aerospace Engineering, S.Hickel@tudelft.nl.

The models used in state-of-the-art computational fluid dynamics (CFD) solvers generally capable of simulating the aforementioned phenomena vary considerably. Choices need to be made on the thermodynamic database, the treatment of thermal nonequilibrium effects, the transport properties modelling, and the approach for handling GSI. As important quantities of interest, such as surface heat fluxes, are highly sensitive to the modelling approaches, large discrepancies between the results obtained with hypersonic CFD codes are common [1, 2].

Another difficulty faced is the choice of a numerical scheme and a computational grid capable of accurately simulating strong shock waves and boundary layers. Most solvers used for these applications employ body-conforming structured grids [1, 3, 4]. Generating these types of grids usually involves strenuous effort from the user especially for detailed features and incremental geometry updates. Unstructured grids have also been employed, however issues affecting the heat flux predictions at the surface were reported [5, 6]. A promising alternative is the use of adaptive mesh refinement techniques based on Cartesian grids with immersed boundary methods (IBM), which offer a relatively straight-forward implementation of high-order schemes. There has been a recently growing interest in IBM solvers [7–11], mainly for their potential for complex and deforming geometries. Especially for boundaries under motion, immersed boundary methods are much more robust and efficient compared to the body-conformal approach. Nevertheless, special care must be taken to have sufficient grid resolution near the boundaries, as it is inherently more difficult for immersed boundary methods to resolve thin boundary layers efficiently.

This paper presents a comparison of three atmospheric entry analysis tools through several relevant verification and validation cases. In line with the preceding discussion, a consistent comparison to assess the performance and accuracy of the numerical methods is achieved by coupling all three solvers to the same thermochemistry library, Mutation++ [12]. Results obtained with the Cartesian grid immersed boundary finite volume solvers INCA from Delft University of Technology and CHESS from Politecnico di Bari are compared to the ones obtained with the reference body-conforming finite volume solver US3D from the University of Minnesota. Governing equations and modelling approaches are presented in Section II. Results of the case studies are discussed in Section III, and concluding remarks are made in Section IV.

II. Governing Equations and Models

The compressible Navier-Stokes equations are solved in their conservative form for a reacting multicomponent fluid,

$$\frac{\partial \rho_i}{\partial t} + \boldsymbol{\nabla} \cdot (\rho_i \mathbf{u} + \mathbf{J}_i) = \dot{\omega}_i \,, \tag{1}$$

$$\frac{\partial \rho \mathbf{u}}{\partial t} + \boldsymbol{\nabla} \cdot (\rho \mathbf{u} \otimes \mathbf{u}) + \boldsymbol{\nabla} p = \boldsymbol{\nabla} \cdot \boldsymbol{\tau} \,, \tag{2}$$

$$\frac{\partial \rho E}{\partial t} + \boldsymbol{\nabla} \cdot \left[(\rho E + p) \, \mathbf{u} \right] + \boldsymbol{\nabla} \cdot \mathbf{q} = \boldsymbol{\nabla} \cdot (\boldsymbol{\tau} \cdot \mathbf{u}) \,. \tag{3}$$

Here, ρ_i is the species partial density for the ith species, $\mathbf{u}$ is the mixture average velocity, $\mathbf{J}_i$ is the species diffusion flux, and $\dot{\omega}_i$ is the source term associated with the production or consumption of species due to chemical reactions. Moreover, ρ is the mixture density, p is the mixture pressure, and $E = e + u^2/2$ is the specific total energy, which is the sum of the thermodynamic internal energy e and the kinetic energy. The viscous stress tensor $\boldsymbol{\tau}$ and the total heat flux $\mathbf{q}$ are detailed below. External forces due to gravitational or magnetic effects, and radiative energy exchanges are not considered for the cases in this study. All three solvers can perform under thermal nonequilibrium with multi-temperature methods, such as that of Park [13]. However, results presented in this paper are obtained with a thermal equilibrium assumption.

The viscous stress tensor is defined assuming Stokes' hypothesis as

$$\boldsymbol{\tau} = \mu \left[\boldsymbol{\nabla} \mathbf{u} + (\boldsymbol{\nabla} \mathbf{u})^\dagger - \frac{2}{3} \boldsymbol{\nabla} \cdot \mathbf{u} \boldsymbol{I} \right] \,, \tag{4}$$

where μ is the dynamic (shear) viscosity of the mixture.

The heat flux term includes the contributions from conduction and mass diffusion,

$$\mathbf{q} = -\lambda \boldsymbol{\nabla} T + \sum_i h_i(T) \rho_i \boldsymbol{\mathcal{V}}_i \,, \tag{5}$$

where T is the temperature. The first term stems from Fourier's law with the thermal conductivity λ of the mixture, and the second term refers to the diffusion of enthalpy with h_i as the species enthalpy and $\boldsymbol{\mathcal{V}}_i$ as the diffusion velocity.

The ideal gas assumption leads to the equation of state $p = \rho R T$, where $R = \mathcal{R}/\overline{M}$ is the mixture gas constant with the universal gas constant $\mathcal{R}$ and mixture average molar mass $\overline{M}$. These mixture properties are obtained according to Dalton's law through their constituent species as $p = \sum_i p_i$, $\rho = \sum_i \rho_i$, $R = \sum_i y_i R_i$, with the mass fractions $y_i = \rho_i/\rho$.

A. Solver Methodologies

1. US3D solver

US3D is a high-fidelity flow solver specifically designed for aerodynamic applications in the hypersonic regime [5]. It solves compressible chemically reacting Navier-Stokes equations in a finite-volume framework on structured or unstructured body-conforming grids. While several low dissipation numerical schemes are available, all simulations carried out within this work made use of the modified Steger-Warming scheme [14], which is suitable for steady computations. A MUSCL approach [15] is employed to obtain second-order accurate fluxes. Both explicit and implicit time integration methods are available; in this work, rapid convergence to steady state was achieved with the Data Parallel Line Relaxation (DPLR) method [16].

US3D is equipped with routines for the closure of chemistry/multi-temperature source terms, transport properties, as well as turbulence models, with the possibility to account for high temperature and high pressure effects.

2. INCA solver

INCA is a high-fidelity finite-volume solver for the compressible chemically reacting Navier-Stokes equations and provides a large number of different discretization schemes on three-dimensional block-Cartesian AMR grids [17, 18]. For the purposes of this study, a third-order weighted essentially non-oscillatory (WENO) scheme [19] with HLLC flux function [20] is selected to discretize the inviscid terms. WENO schemes permit high accuracy in smooth regions, while ensuring stable and sharp capturing of discontinuities. Second-order centered differences are used for the viscous terms and the explicit third-order Runge-Kutta scheme of Gottlieb and Shu [21] is selected for time integration.

INCA provides a cut-element based immersed boundary method, which is a consistent and conservative extension of the finite volume flux balance to accommodate cells being split by boundaries [22, 23]. This method is based on representing the fluid-solid interface through cut-elements, which are derived from an STL triangulation of the surface geometry to yield sub-cell accuracy. Instead of considering an average planar geometry to approximate the body shape as in the level-set technique, cut-elements are formed from the intersection of the grid with the geometrical triangulation. The interface within each cut-cell is thus represented by several cut-elements belonging to different triangles. The exchange of mass (e.g. with surface reactions), momentum, and energy through these cut-elements is calculated from the prescribed boundary conditions and local fluid values at a point within the fluid domain, which is generally a half cell length away from the interface. The value of a quantity of interest at this fluid point is acquired by interpolation from the surrounding cell values and the boundary conditions. Ghost-cells are employed to allow for the use of unmodified stencils throughout the domain.

Chemical source terms are treated using Strang's second-order accurate time splitting scheme [24] to alleviate the numerical stiffness caused by these terms. The chemical source terms reduce to a system of ordinary differential equations (ODE), which is solved by the VODE library [25].

3. CHESS solver

CHESS (Cuda HypErSonic Solver) is a finite-volume body-conforming solver developed at Politecnico di Bari. It is able to solve high temperature flows past several geometries (cylinder, sphere, double-wedge and others). The numerical scheme is based on the flux vector splitting proposed by Steger and Warming [14], combined with a second-order MUSCL reconstruction in space [15], for the advection terms. Diffusive fluxes are discretized using Gauss' theorem and a second-order linear reconstruction of the solution. Time integration is performed through a third-order explicit Runge-Kutta scheme. The algorithm is able to solve both steady and unsteady flows. The chemical source terms are evaluated through a splitting approach. In a first step, the system of homogeneous Navier-Stokes equations is solved. After the Runge-Kutta time integration, chemical source terms are computed by means of a Gauss-Seidel iterative scheme.

In order to simulate flows past complex geometries, the solver has been extended to include an IBM algorithm, which employs a linear reconstruction for the flow variables. The algorithm is based on a local refinement strategy to increase accuracy near the wall [26].

B. Mutation⁺⁺ Library Coupling

MUlticomponent Thermodynamic And Transport properties for IONized gases in C++ (Mutation⁺⁺) library is utilized in all the solvers to provide closure to the governing equations. A detailed description of Mutation⁺⁺ is presented by Scoggins et al. [12]. Fundamentally, it consists of four modules for thermodynamics, transport properties, chemical kinetics, and GSI.

INCA and CHESS solvers use the thermodynamic databases provided by Mutation⁺⁺, whereas US3D uses its own native routines. For consistency, all solvers use NASA-9 polynomial fits [27].

In terms of transport properties, all solvers use multicomponent Chapman-Enskog formulations. Viscosity and thermal conductivity are obtained through a linear system solution using an LDL$^\mathrm{T}$ decomposition as opposed to the common approach of using simplified mixture rules [28–30]. Mutation⁺⁺ can provide mass diffusivities for the modified Fick's law expression

$$\mathbf{J}_i = -\rho D_{im} \boldsymbol{\nabla} y_i \quad \text{with} \quad D_{im} = \frac{1 - x_i}{\sum_{j \neq i} \frac{x_j}{\mathscr{D}_{ij}}} \, , \tag{6}$$

such that the mixture-averaged diffusion coefficients D_{im} are obtained by Wilke's averaging of the binary diffusion coefficients $\mathscr{D}_{ij}$. These fluxes are then corrected to ensure conservation of mass. This version of the modified Fick's law is used by INCA and CHESS. On the other hand, US3D uses Stefan-Maxwell equations,

$$\boldsymbol{\nabla} x_i = \frac{\overline{M}}{\rho} \sum_{j \neq i} \left(\frac{x_i \mathbf{J}_j}{M_j \mathscr{D}_{ij}} - \frac{x_j \mathbf{J}_i}{M_i \mathscr{D}_{ij}} \right) \, , \tag{7}$$

where x_i are the mole fractions, and M_i are the species molar masses. This formulation is also available in INCA through Mutation⁺⁺; it is computationally costlier, but considered more accurate [31]. For chemical reactions, mass rates and their analytical Jacobians with respect to species densities are provided by Mutation⁺⁺.

Finally, at catalytic and ablative surface boundaries a mass balance is solved directly by calling Mutation⁺⁺ [12, 32]. It could be written for each species in the following form

$$(\rho_i v)_{wall} + (\rho_i \mathcal{V}_i)_{wall} = \dot{\omega}_{i,wall} \, , \tag{8}$$

with v as the surface normal blowing velocity, which is nonzero for an ablative boundary. Terms from left to right in Eq. (8) refer to convective flux due to blowing, diffusive flux, and a species source term due to surface reactions. A probability based approach is employed for computing this chemical source term for the surface, written as

$$\dot{\omega}_{i,wall} = \gamma m_i \mathcal{F}_{i,impin} \, , \tag{9}$$

where $\gamma = \mathcal{F}_{i,react} / \mathcal{F}_{i,impin}$ is the ratio of reacting to impinging species fluxes and it describes the efficiency of the process, and m_i is the mass of the ith species [32]. Then, from the mass blowing rate $\dot{m} = \sum_i \dot{\omega}_{i,wall}$, the blowing speed is calculated by

$$v_{blow} = \frac{\dot{m}}{\sum_i \rho_i} \, . \tag{10}$$

Values obtained for species densities and mass blowing speeds are then imposed as boundary conditions for the fluid solution.

III. Results

The test cases studied with the three solvers are summarized in Table 1. The first four cases present the verification of chemistry, transport properties, the catalytic boundary condition, and the numerical scheme for shock capturing. Then, two validation cases are considered. Firstly, a 2-D cylinder geometry is studied with inert adiabatic, inert isothermal, and catalytic isothermal surfaces. Then, the second validation case considers an ablative isothermal surface for a probe geometry under plasma wind tunnel conditions.

A. 0-D Reactor

The first study verifies the chemical source term by considering 5-species air, $[N_2, O_2, NO, N, O]$, in an adiabatic box. Starting from the chemical non-equilibrium initialization provided in Table 2, the system is left free to time-march towards the equilibrium state according to chemical mechanisms from Park [33, 34]. The solutions provided by all three solvers are shown in Fig. 1. The code-to-code agreement is excellent between all solvers.

Table 1   Summary of studied cases.

	Name	Aspect to Assess
Section III.A	0-D Reactor	Chemistry
Section III.B	1-D Diffusion Problem	Mass diffusion
Section III.C	1-D Catalytic Diffusion Problem	Mass diffusion with catalysis
Section III.D	1-D Shocktube	Shock capturing
Section III.E	2-D Cylinder	Surface heat flux with catalysis
Section III.F	2-D Ablator	Surface mass blowing with ablation

Table 2   Setup conditions for the 0-D reactor case.

ρ [kg/m^3]	T [K]	u [m/s]	$y(N_2)$	$y(O_2)$
0.01	7000	0.0	0.767	0.233

B. 1-D Diffusion Problem

This test case verifies the models for transport properties. Viscosity and thermal conductivity are obtained through direct calls to Mutation^{++}, and are exactly equal for all solvers. Therefore, mainly the differences in diffusion models are assessed. The setup consists of a 1-D tube with isothermal end walls at different temperatures. The initial and boundary conditions are provided in Table 3. The mixture composition and reaction mechanisms are the same as in the previous case. The tube is 3 mm long.

In this test case the temperature gradient leads to chemical reactions, which in turn drive mass diffusion. Temperature and mass fraction distributions along the tube are presented in Fig. 2. INCA results have been obtained by both Fick's law and Stefan-Maxwell diffusion models. However, for this test case, there seems to negligible difference between the two. Overall, US3D results are matched well with INCA, while slight differences are observed for the mass fraction distributions with CHESS, even though the temperature profiles match exactly. It should be pointed out that the computational mesh in US3D and INCA solvers involved 100 cells, whereas CHESS used 400 cells since a coarser grid was not able to match the temperature profiles.

C. 1-D Catalytic Diffusion Problem

This test case verifies the catalytic boundary condition implementation for a simple [N$_2$, N] binary mixture along a 1-D tube, for which an analytical solution exists and is derived in the appendix. Setup conditions are given in Table 4.
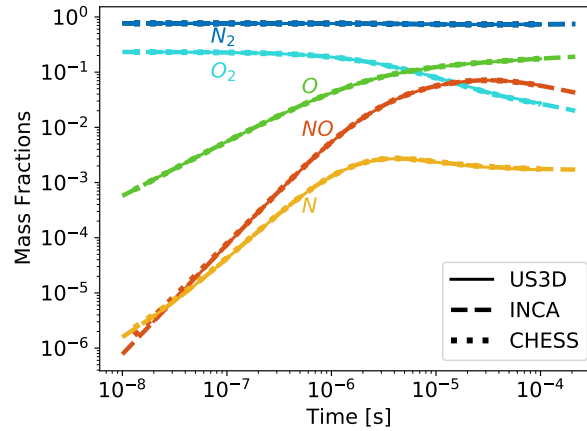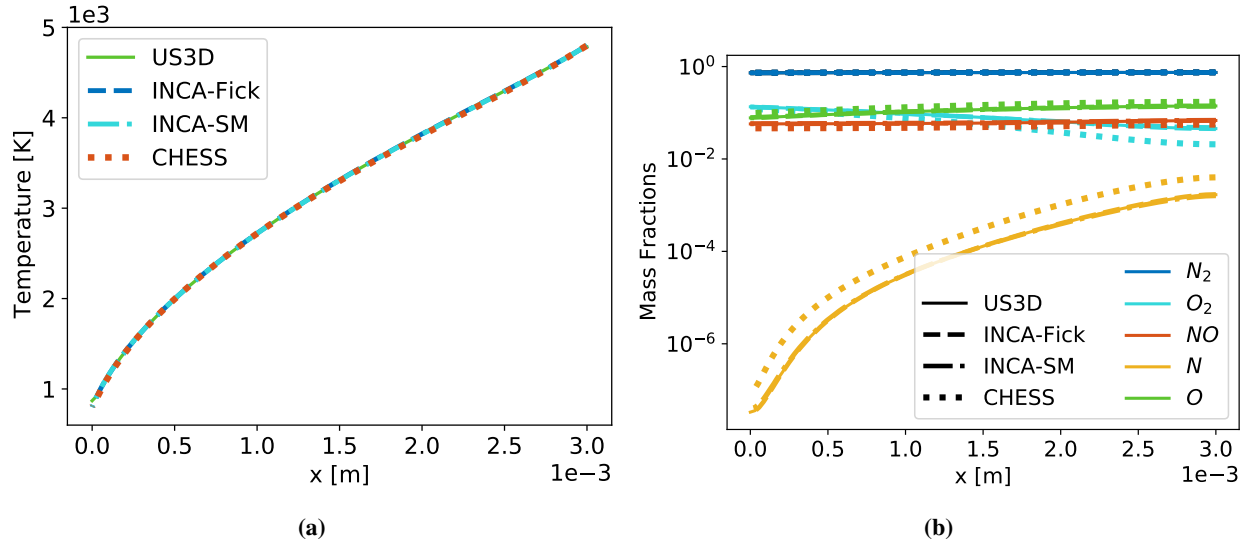

Fig. 1   Evolution of mass fractions for 5-species air in the 0-D reactor case.

Table 3   Setup conditions for the 1-D diffusion case.

ρ [kg/m^3]	T [K]	T_{left} [K]	T_{right} [K]	u [m/s]	$y(N_2)$	$y(O_2)$
0.02	1000	800	4800	0.0	0.767	0.233

(a)   **(b)**

Fig. 2   Comparison of (a) temperature and (b) mass fraction distributions for the 1-D diffusion case.

The length of the tube is 0.2 m. One side of the tube is at reservoir conditions, while at the other, at $x = 0.2$, a catalytic wall is present. Catalytic reactions considered the recombination of nitrogen, $N + N \rightarrow N_2$.

Table 4   Setup conditions for the 1-D catalytic diffusion case.

p [Pa]	T [K]	T_{wall} [K]	u [m/s]	$y(N_2)$	$y(N)$	γ_N
100	3000	3000	0.0	0.0	1.0	[0.001, 0.01, 0.1, 1.0]

Results comparing the analytical solution with the three solvers is given in Fig. 3. Naturally, for higher values of the recombination coefficient γ, the value of molecular nitrogen at the wall increases, and reaches unity for the fully catalytic case. An excellent agreement is present between all the results.

D. 1-D Shocktube

The Riemann problem of Grossman and Cinnella [35] is used to evaluate shock capturing. The unit domain is spatially discretized by 600 cells, in line with the reference resolution. The diaphragm separating the two states is set at the midpoint of the tube. The initial conditions for the two states are given in Table 5. 5-species air is considered. The reaction mechanism is taken from an earlier work of Park [36], to match with the reference. Although the original case is with thermal nonequilibrium, here thermal equilibrium is assumed. Preliminary tests using Park's two-temperature model [13] showed no significant differences between the translational and vibrational energy modes.

The state of the shocktube after 99 μs in terms of pressure and density is shown in Fig. 4, and mass fractions are given in Fig. 5. The contact discontinuity and the shock wave traveling in the positive x direction and the expansion traveling in the opposite direction are well captured. The peak in density after the shock also matches perfectly with the reference results without any oscillations. Mass fractions show minor differences, but the overall agreement is satisfactory for all three solvers.
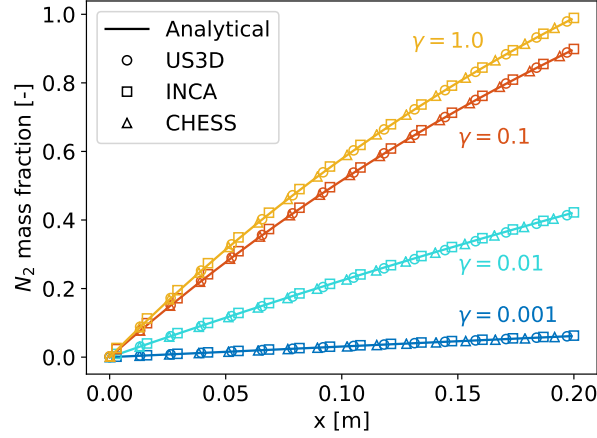
6

Fig. 3 **N$_2$ mass fractions for different recombination coefficients γ for the 1-D catalytic diffusion problem.**

Table 5 **Setup conditions for the 1-D shocktube case.**

u_1 [m/s]	T_1 [K]	p_1 [Pa]	u_2 [m/s]	T_2 [K]	p_2 [Pa]
0.0	9000	195256	0.0	300	10000

E. 2-D Cylinder

This test case considers the validation of surface heat flux calculations under inert and catalytic wall conditions. Knight et al. [1] have presented an assessment of five different CFD codes from participating institutions with respect to experiments conducted at the high-enthalpy shock tunnel of the German Aerospace Center (DLR). The experiment involves the flow past a cylinder with a radius of 0.045 m exposed to a reported total enthalpy of 22.4 MJ/kg. The experimental setup is replicated by imposing the freestream conditions given in Table 6 and Table 7 on the left boundary. Symmetry is imposed along the stagnation line, and the outer boundaries are set as supersonic outlets. The reaction mechanism employed for the 5-species air model is taken from Park [33, 34]. Three different surface conditions are tested in the following sections: two inert cases with adiabatic and isothermal conditions, and a third one with a fully catalytic isothermal wall.

Table 6 **Freestream conditions for the 2-D cylinder case.**

M$_\infty$	u_∞ [m/s]	T_∞ [K]	p_∞ [Pa]	ρ_∞ [kg/m^3]
8.98	5956	901	476	1.547×10^{-3}

1. Inert Adiabatic Wall

For the adiabatic wall, the temperature and species mass fractions along the stagnation line are presented in Fig. 6. Shock stand-off distance and the dissociation of molecular nitrogen and oxygen in the shock layer are predicted in good agreement between all solvers. As it was indicated by the previous verification cases, major modules provided by Mutation^{++} produced the same outputs from these different solvers. This case confirms once more that the baseline implementations of Mutation^{++} have been carried out correctly in all the solvers.

2. Inert Isothermal Wall

An isothermal wall boundary condition with a wall temperature of 300 K is imposed on the cylinder surface, in accordance with the specifications by Knight et al. [1].

Stagnation line temperature and mass fraction distributions are plotted in Fig. 7. For both quantities, INCA and
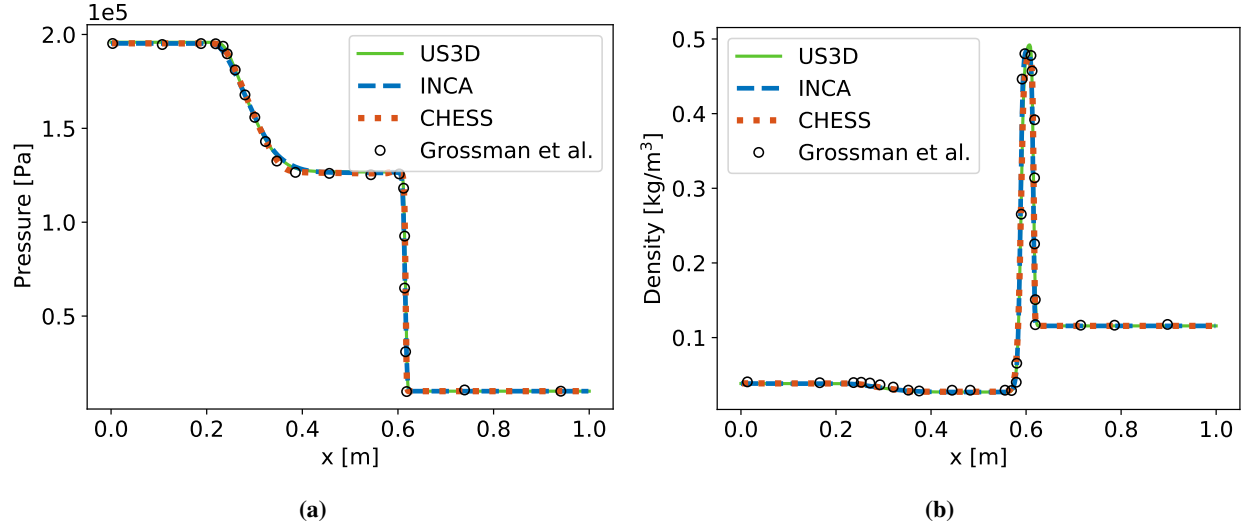
7

Fig. 4   Comparison of (a) pressure and (b) density distributions for the 1-D shocktube case.
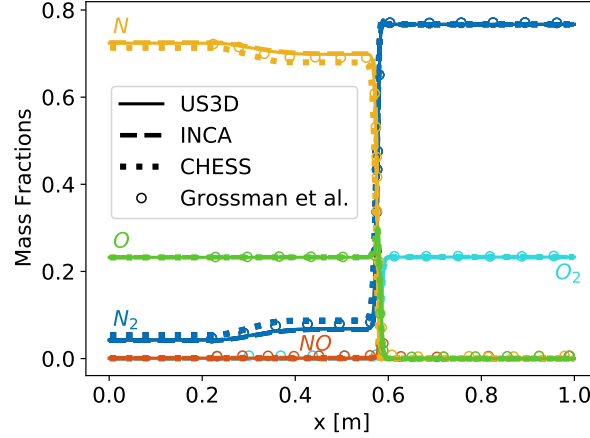

Fig. 5   Comparison of mass fraction distributions for the 1-D shocktube case

US3D match almost exactly, including the steep temperature and species variations in the boundary layer. Results from CHESS, on the other hand, suffer from a misprediction of the shock stand-off distance, which in turn affects the whole flow field. This could be attributed to the ghost-point immersed boundary methodology adopted by CHESS, which is known to be nonconservative. Mass conservation errors manifest as an unphysical blowing from the surface. Consequently, the shock stand-off distance is increased. The adiabatic case is less affected by this defect, as it does not involve large temperature gradients near the wall. This discrepancy is not observed with INCA, where conservation is ensured along the immersed boundary with the cut-element based sharp interface approach.

In Fig. 8, surface pressure and heat flux distributions are compared with the experimental values from Knight et al. [1] and also with the numerical simulations of Nompelis from the same publication. All three solvers show an excellent agreement for the pressure distributions. As for the heat fluxes, results from INCA and US3D are in very good agreement and match with the experimental measurements and perform better than the numerical simulations of Nompelis. Slight differences in heat fluxes are expected to be due to the differences in grid resolutions at the surface. The smallest cell size near the wall is 1.0×10^{-8} m for US3D, 1.25×10^{-6} m for INCA, and 1.0×10^{-6} m for CHESS. For this case, CHESS is not able to calculate the heat flux correctly. This is expected due to the aforementioned shortcomings in its nonconservative IBM. A similar underprediction has also been reported in literature by Brahmachary et al. [11], where the issue has been linked to the reconstruction of temperature by linear interpolation. We would like to remark that since INCA is also following a similar approach for reconstructing these variables, the larger source of error

Table 7   Freestream species mass fractions for the 2-D cylinder case.

$y(N_2)$	$y(O_2)$	$y(NO)$	$y(N)$	$y(O)$
0.7543	0.00713	0.01026	6.5×10^{-7}	0.2283
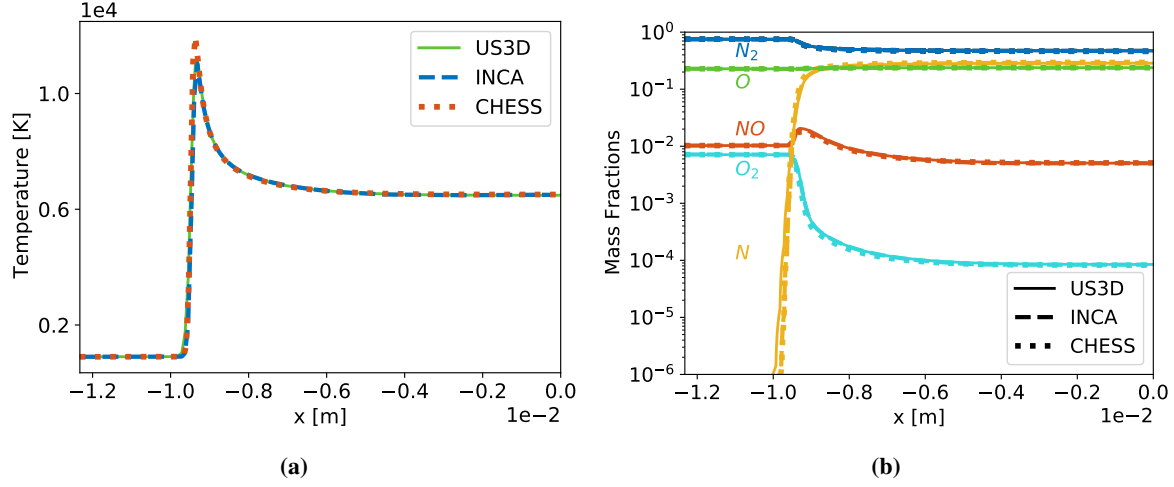
Fig. 6   Comparison of (a) temperature and (b) mass fractions along the stagnation line for the inert adiabatic 2-D cylinder case.
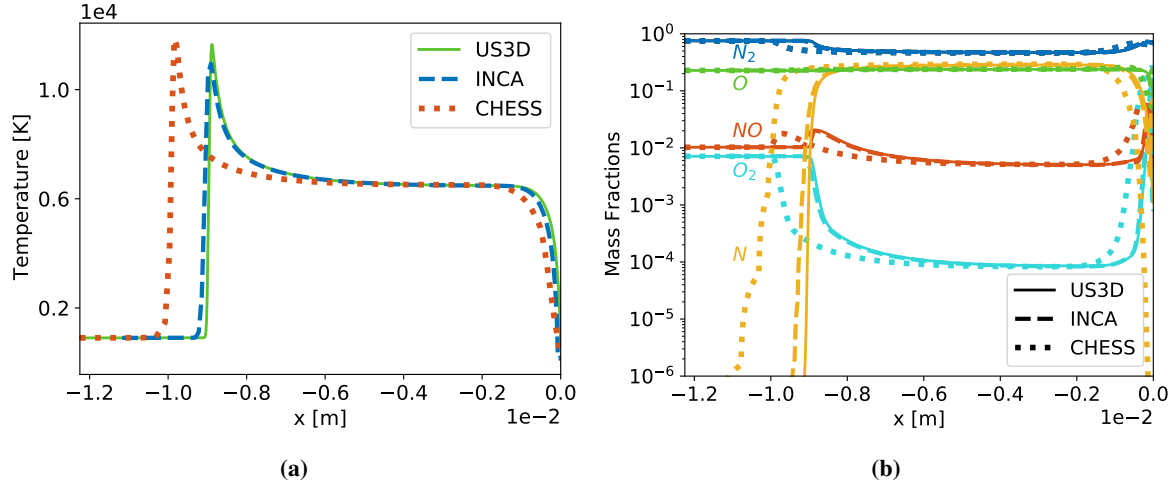
Fig. 7   Comparison of (a) temperature and (b) mass fractions along the stagnation line for the inert isothermal 2-D cylinder case.

is still attributed to the nonconservative nature of the IBM.

3. Catalytic Isothermal Wall

As the third cylinder case, a fully catalytic wall ($\gamma = 1.0$) at the same temperature of 300 K is considered. Nompelis [1] have found that this catalytic boundary condition leads to a better agreement with the experiments. This type of reactive surface imposes the recombination of all atoms impinging on the surface. Due to this exothermic process, the surface heat flux is enhanced through diffusive heat flux.

Results are shown in Fig. 9 for the species mass fractions close to the wall along the stagnation line and the total
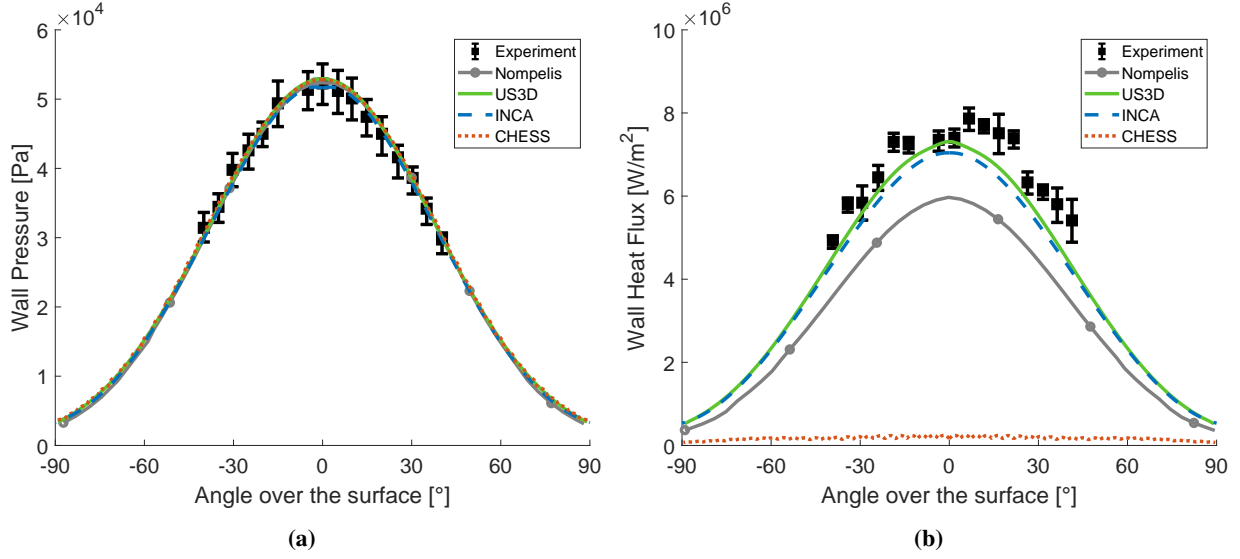
9

Fig. 8   Comparison of surface (a) pressures and (b) heat fluxes for the inert isothermal 2-D cylinder case.
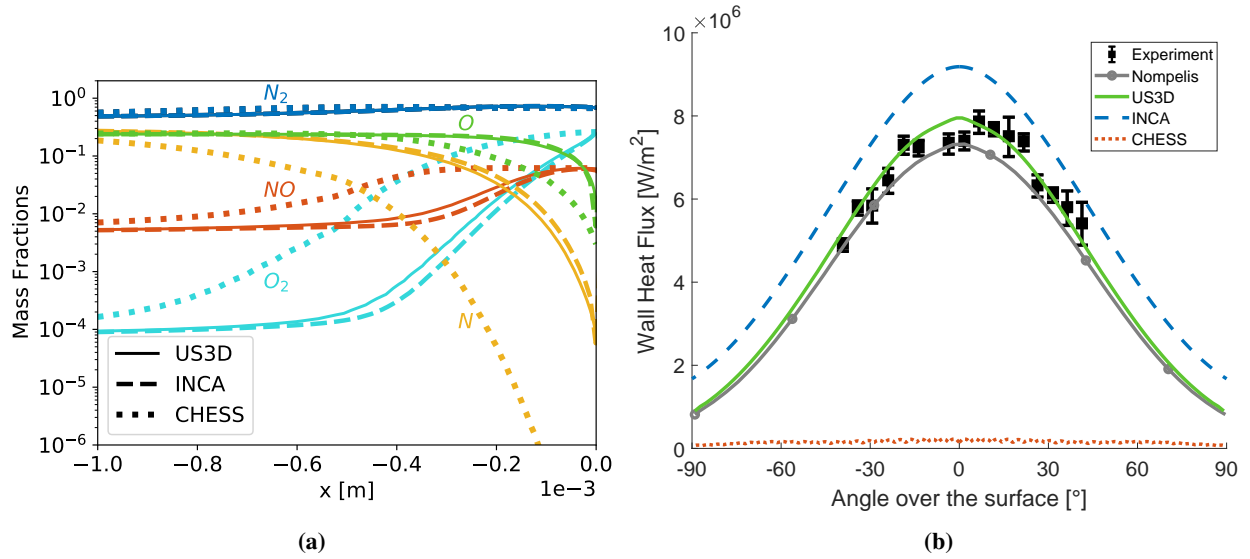

Fig. 9   Comparison of (a) mass fractions along the stagnation line and (b) heat fluxes over the surface for the catalytic isothermal 2-D cylinder case.

surface heat flux distributions. Our previous comments for the inert isothermal case apply here as well regarding the differences seen in the results of the CHESS solver. INCA is shown to agree satisfactorily with the US3D results in terms of species distributions. However, it is observed that with the introduction of the diffusive heat flux, INCA predicts a higher heat flux over the surface than Nompelis and the experiment. As remarked by Knight et al. [1], there appears to be a large variation in the results from different solvers, especially regarding the treatment of the surface. It is suspected that the fully catalytic conditions were only achieved for a short duration at the beginning of the experiment. However, since the cold wall itself is already enough to excite a sufficient degree of recombination in the boundary layer, catalysis should probably not cause such a major increase as predicted by the INCA solver. Since the verification of the implementation was successful, the immersed boundary treatment with catalysis is currently being investigated for any anomalies.

10

F. 2-D Ablator

To validate the ablative boundary condition implementation, a subsonic plasma wind tunnel experiment conducted at the von Karman Institute by Helber et al. [37] is considered. The experiment exposes a graphite sample with a hemispherical nose of radius 25 mm to nitrogen plasma. The sample undergoes ablation through nitridation reactions

$$C_{(solid)} + N \rightarrow CN \,, \tag{11}$$

with the reaction probability

$$\gamma = 7.91 \cdot 10^{-2} \exp\left(-\frac{5663}{T_{wall}}\right) \,. \tag{12}$$

The nitridation efficiency was calibrated based on this particular experiments [37]. Recession of the sample is not studied.

Firstly, the experiment is reproduced by the US3D solver including the support structure extending towards the back of the sample by 250 mm. For these simulations with an axisymmetric geometry, a 9-species nitrogen-carbon mixture is considered, including free electrons and ionized species. These simulations yielded a stagnation point mass blowing rate of 0.003 41 kg/m^{2}s, which is within the experimental uncertainty range set by 0.0028864 ∓ 0.000965 kg/m^{2}s. This serves to validate the mass blowing rates through Mutation^{++} with US3D before the comparison with the other solvers.

Having confidence in the US3D solver implementation, the experimental test case is simplified to a 2-D geometry without ionized species to reduce the computational cost and to avoid straying too far from the objective to validate the ablative boundary condition. Hence, this ablative case should be seen as a consistent successor of the catalytic validation campaign, that is, even though the conditions are different, the numerical specifications remain similar. Freestream conditions of this 2-D case are given in Table 8. A 6-species mixture of [N$_2$, N, CN, C$_3$, C$_2$, C] is considered. Grid resolutions at the wall for all solvers are fixed at 1×10^{-5} m.

Table 8   Freestream conditions for the 2-D ablator case.

u_∞ [m/s]	T_∞ [K]	T_{wall} [K]	p_∞ [Pa]	$y(N_2)$	$y(N)$
1570	10280	2407	1500	9.77659e-05	0.9999022341

The mass fractions along the stagnation line and the mass blowing rates over the wall are shown in Fig. 10. Mass fractions for C$_3$ are not seen as they are almost zero. Species mass fractions for US3D and INCA agree well with each other. The ones from CHESS indicate lower values for all species except atomic nitrogen. Overall, the production of CN at the wall and the dissociation of it through gas-phase reactions to form atomic nitrogen are well captured. Mass blowing rates from US3D and INCA also show very good agreement with slightly higher values for INCA, which is consistent with the catalytic validation case. CHESS results predict a higher mass blowing rate, yet still perform well in capturing the overall trend.

IV. Conclusion

Verification and validation results of two IBM solvers, INCA and CHESS, in relevant conditions for atmospheric entry are presented. Results are compared with those obtained with a body-conforming solver, US3D, which is coupled to the same external thermochemistry library, Mutation^{++}, as the IBM solvers.

In these campaigns, the INCA solver has shown an almost perfect agreement with the body-conforming solver and reference results. Small differences were mainly seen in diffusive heat fluxes and mass blowing rates. These will be further investigated in future studies. The CHESS solver has also performed sufficiently, capturing the main trends in all of the test campaigns. The major issue that was observed with this solver is attributed to conservation errors of the IBM algorithm used by CHESS, which can have a large effect in the presence of strong gradients. These issues are currently under investigation.

Solvers employing IBM offer promising advantages, but the accuracy of the numerical schemes used for predicting surface quantities must be analyzed rigorously. Overall, the benefit of an IBM that strictly conserves mass, momentum, and energy, such as the cut-element method in INCA, is crucial. It is clear that simulating these complex flows still involves significant uncertainties regarding surface boundary conditions. We remark that the selection of a set of well defined test cases by mutual collaboration between research groups is crucial in converging to a scientific consensus on
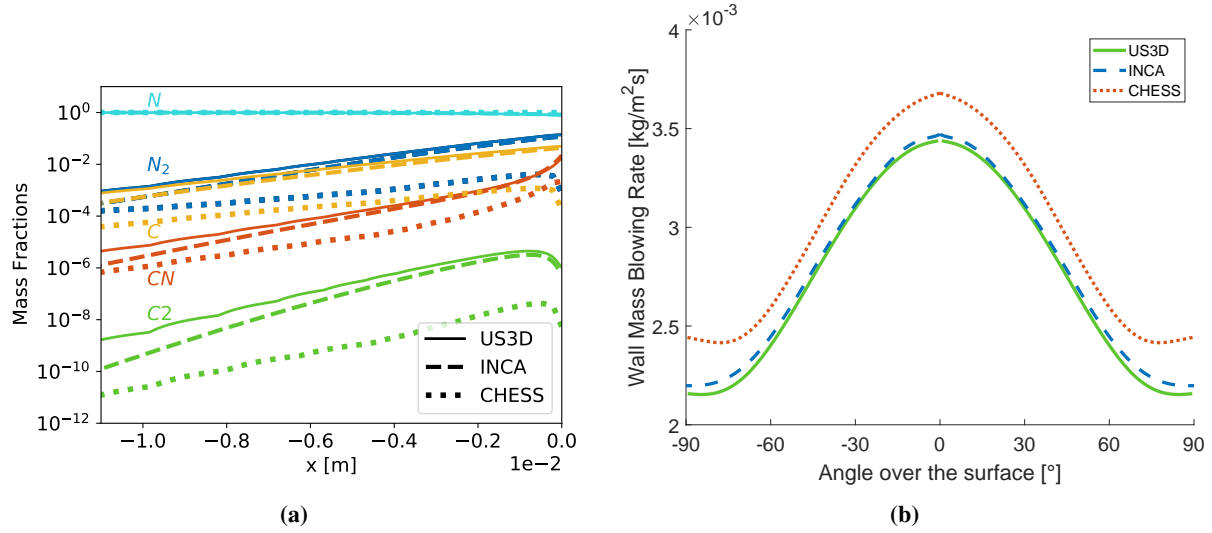
(a)

(b)

Fig. 10   Comparison of (a) mass fractions along the stagnation line and (b) mass blowing rates over the surface for the 2-D ablator case.

the prediction of these surface states. To that end, this paper establishes such a set of fundamental verification and validation cases to assess the performance of solvers and models for reacting surfaces under conditions relevant to atmospheric entry.

Appendix

Analytical Solution of the 1-D Catalytic Diffusion Problem

Following the derivation proposed by Bariselli [38], plugging Fick's law into the molar continuity equation, and looking for the zero-advection, constant temperature, steady-state solution one obtains

$$\nabla \cdot \left(n \frac{M_N}{\overline{M}} D_{N_2,N} \nabla(x_{N_2})\right) = 0 \,, \tag{13}$$

with n as the number density. For the current binary mixture $M_{N_2} = 2M_N$ and $\overline{M} = \sum_i x_i M_i$, which in 1-D leads to

$$\frac{d}{d\eta}\left(\frac{1}{x_{N_2}+1}\left(\frac{d}{d\eta}x_{N_2}\right)\right) = 0 \,, \tag{14}$$

with η as the spatial coordinate. Solving for x_{N_2} yields

$$x_{N_2} = \frac{e^{C_1 M_N \eta} e^{C_2 M_N}}{M_N} \,, \tag{15}$$

with C_1 and C_2 as integration constants to be found through the boundary conditions at the free-stream reservoir

$$X_{N_2}|_{\eta=0} = 0 \rightarrow C_2 = \frac{\ln M_N}{M_N} \,, \tag{16}$$

and by equating the diffusion flux to the chemical production rate at the wall

$$(J_{N_2} = \dot{\omega}_{N_2})_{\eta=L} \rightarrow \left(\frac{C_1 M_N}{2 - e^{C_1 L M_N}} = \frac{\gamma_N}{2 D_{N_2 N}} \sqrt{\frac{k_B T}{2\pi m_N}}\right)|_{\eta=L} \,, \tag{17}$$

where k_B stands for the Boltzmann constant. The last expression could be solved iteratively through the Newton-Raphson method. The solution describes the species distribution as a function of spatial variable η.

12

References

[1] Knight, D., Longo, J., Drikakis, D., Gaitonde, D., Lani, A., Nompelis, I., Reimann, B., and Walpot, L., "Assessment of CFD capability for prediction of hypersonic shock interactions," *Progress in Aerospace Sciences*, Vol. 48, 2012, pp. 8–26.

[2] Alkandry, H., Boyd, I., and Martin, A., "Comparison of models for mixture transport properties for numerical simulations of ablative heat-shields," *51st AIAA Aerospace Sciences Meeting including the New Horizons Forum and Aerospace Exposition*, 2013, p. 303.

[3] Wright, M. J., White, T., and Mangini, N., *Data Parallel Line Relaxation (DPLR) Code User Manual: Acadia Version 4.01. 1*, National Aeronautics and Space Administration, Ames Research Center, 2009.

[4] Knight, D., Chazot, O., Austin, J., Badr, M. A., Candler, G., Celik, B., de Rosa, D., Donelli, R., Komives, J., Lani, A., et al., "Assessment of predictive capabilities for aerodynamic heating in hypersonic flow," *Progress in Aerospace Sciences*, Vol. 90, 2017, pp. 39–53.

[5] Candler, G. V., Johnson, H. B., Nompelis, I., Gidzak, V. M., Subbareddy, P. K., and Barnhardt, M., "Development of the US3D code for advanced compressible and reacting flow simulations," *53rd AIAA Aerospace Sciences Meeting*, 2015, p. 1893.

[6] Scalabrin, L., and Boyd, I., "Development of an unstructured Navier-Stokes solver for hypersonic nonequilibrium aerothermo-dynamics," *38th AIAA Thermophysics Conference*, 2005, p. 5203.

[7] Sekhar, S. K., and Ruffin, S. M., "Predictions of Convective Heat Transfer Rates using a Cartesian Grid Solver for Hypersonic Flows," *44th AIAA Thermophysics Conference*, 2013, p. 2645.

[8] Atkins, C., and Deiterding, R., "Towards a Strand-Cartesian Solver for Modelling Hypersonic Flows in Thermochemical Non-Equilibrium," *23rd AIAA International Space Planes and Hypersonic Systems and Technologies Conference*, 2020.

[9] McQuaid, J. A., Zibitsker, A. L., Saikia, B., Martin, A., and Brehm, C., "An Immersed Boundary Method for Hypersonic Viscous Flows," *AIAA Scitech 2021 Forum*, 2021, p. 0926.

[10] Fu, R., and Martin, A., "Hinge Method For CFD and Fluid-Ablation Interaction Modeling," *AIAA AVIATION 2021 FORUM*, 2021, p. 3132.

[11] Brahmachary, S., Natarajan, G., Kulkarni, V., Sahoo, N., Ashok, V., and Kumar, V., "Role of solution reconstruction in hypersonic viscous computations using a sharp interface immersed boundary method," *Physical Review E*, Vol. 103, No. 4, 2021, p. 043302.

[12] Scoggins, J. B., Leroy, V., Bellas-Chatzigeorgis, G., Dias, B., and Magin, T. E., "Mutation++: Multicomponent thermodynamic and transport properties for ionized gases in C++," *SoftwareX*, Vol. 12, 2020, p. 100575.

[13] Park, C., *Nonequilibrium hypersonic aerothermodynamics*, 1989.

[14] Steger, J. L., and Warming, R., "Flux vector splitting of the inviscid gasdynamic equations with application to finite-difference methods," *Journal of Computational Physics*, Vol. 40, No. 2, 1981, pp. 263–293.

[15] Van Leer, B., "Towards the ultimate conservative difference scheme. V. A second-order sequel to Godunov's method," *Journal of Computational Physics*, Vol. 32, No. 1, 1979, pp. 101–136.

[16] Wright, M. J., Candler, G. V., and Bose, D., "Data-Parallel Line Relaxation Method for the Navier-Stokes Equations," *AIAA Journal*, Vol. 36, No. 9, 1998, pp. 1603–1609.

[17] Hickel, S., Egerer, C. P., and Larsson, J., "Subgrid-scale modeling for implicit large eddy simulation of compressible flows and shock-turbulence interaction," *Physics of Fluids*, Vol. 26, No. 10, 2014, p. 106101.

[18] Müller, H., Niedermeier, C. A., Matheis, J., Pfitzner, M., and Hickel, S., "Large-eddy simulation of nitrogen injection at trans-and supercritical conditions," *Physics of fluids*, Vol. 28, No. 1, 2016, p. 015102.

[19] Jiang, G.-S., and Shu, C.-W., "Efficient implementation of weighted ENO schemes," *Journal of Computational Physics*, Vol. 126, No. 1, 1996, pp. 202–228.

[20] Toro, E. F., *Riemann solvers and numerical methods for fluid dynamics: a practical introduction*, Springer Science & Business Media, 2013.

[21] Gottlieb, S., and Shu, C.-W., "Total variation diminishing Runge-Kutta schemes," *Mathematics of Computation*, Vol. 67, No. 221, 1998, pp. 73–85.

[22] Örley, F., Pasquariello, V., Hickel, S., and Adams, N. A., "Cut-element based immersed boundary method for moving geometries in compressible liquid flows with cavitation," *Journal of Computational Physics*, Vol. 283, 2015, pp. 1–22.

[23] Pasquariello, V., Hammerl, G., Örley, F., Hickel, S., Danowski, C., Popp, A., Wall, W. A., and Adams, N. A., "A cut-cell finite volume–finite element coupling approach for fluid–structure interaction in compressible flow," *Journal of Computational Physics*, Vol. 307, 2016, pp. 670–695.

[24] Strang, G., "On the construction and comparison of difference schemes," *SIAM Journal on Numerical Analysis*, Vol. 5, No. 3, 1968, pp. 506–517.

[25] Brown, P. N., Byrne, G. D., and Hindmarsh, A. C., "VODE: A variable-coefficient ODE solver," *SIAM Journal on Scientific and Statistical Computing*, Vol. 10, No. 5, 1989, pp. 1038–1051.

[26] de Tullio, M. D., De Palma, P., Iaccarino, G., Pascazio, G., and Napolitano, M., "An immersed boundary method for compressible flows using local grid refinement," *Journal of Computational Physics*, Vol. 225, No. 2, 2007, pp. 2098–2117.

[27] McBride, B., Zehe, M., and Gordon, S., "NASA Glenn coefficients for calculating thermodynamic properties of individual species," 2002.

[28] Wilke, C., "A viscosity equation for gas mixtures," *The Journal of Chemical Physics*, Vol. 18, No. 4, 1950, pp. 517–519.

[29] Mason, E., and Saxena, S., "Approximate formula for the thermal conductivity of gas mixtures," *The Physics of Fluids*, Vol. 1, No. 5, 1958, pp. 361–369.

[30] Sarma, G., "Physico–chemical modelling in hypersonic flow simulation," *Progress in Aerospace Sciences*, Vol. 36, No. 3-4, 2000, pp. 281–349.

[31] Sutton, K., and Gnoffo, P., "Multi-component diffusion with application to computational aerothermodynamics," *7th AIAA/ASME Joint Thermophysics and Heat Transfer Conference*, 1998, p. 2575.

[32] Bellas Chatzigeorgis, G., Turchi, A., Viladegut, A., Chazot, O., Barbante, P. F., and Magin, T., "Development of catalytic and ablative gas-surface interaction models for the simulation of reacting gas mixtures," *23rd AIAA Computational Fluid Dynamics Conference*, 2017, p. 4499.

[33] Park, C., "Review of chemical-kinetic problems of future NASA missions. I-Earth entries," *Journal of Thermophysics and Heat transfer*, Vol. 7, No. 3, 1993, pp. 385–398.

[34] Park, C., Jaffe, R. L., and Partridge, H., "Chemical-kinetic parameters of hyperbolic earth entry," *Journal of Thermophysics and Heat transfer*, Vol. 15, No. 1, 2001, pp. 76–90.

[35] Grossman, B., and Cinnella, P., "Flux-split algorithms for flows with non-equilibrium chemistry and vibrational relaxation," *Journal of Computational Physics*, Vol. 88, No. 1, 1990, pp. 131–168.

[36] Park, C., "On convergence of computation of chemically reacting flows," *23rd Aerospace Sciences Meeting*, 1985, p. 247.

[37] Helber, B., Turchi, A., and Magin, T. E., "Determination of active nitridation reaction efficiency of graphite in inductively coupled plasma flows," *Carbon*, Vol. 125, 2017, pp. 582–594.

[38] Bariselli, F., Torres, E., and Magin, T. E., "State-specific catalytic recombination boundary condition for DSMC methods in aerospace applications," *AIP Conference Proceedings*, Vol. 1786, No. 1, 2016, p. 190009. https://doi.org/10.1063/1.4967687, URL https://aip.scitation.org/doi/abs/10.1063/1.4967687.